

# **DFT insights into the bonding mechanism of five-membered aromatic heterocycles containing N, O, or S on Fe(110) surface**

Thong Le Minh Pham<sup>a,b\*</sup>, Thanh Khoa Phung<sup>c,d</sup>, Ho Viet Thang<sup>e</sup>

<sup>a</sup>*Institute of Research and Development, Duy Tan University, Da Nang City 550000, Viet Nam.  
Email: [phamlminhthong@duytan.edu.vn](mailto:phamlminhthong@duytan.edu.vn)*

<sup>b</sup>*Faculty of Environmental and Chemical Engineering, Duy Tan University, Da Nang, 550000, Viet Nam*

<sup>c</sup>*Department of Chemical Engineering, School of Biotechnology, International University, Ho Chi Minh City, Vietnam*

<sup>d</sup>*Vietnam National University, Ho Chi Minh City, Vietnam.*

<sup>e</sup>*The University of Da-Nang, University of Science and Technology, 54 Nguyen Luong Bang, Da-Nang 550000, Vietnam*

Corresponding author: [phamlminhthong@duytan.edu.vn](mailto:phamlminhthong@duytan.edu.vn) (T.L.M.P)

## ABSTRACT

Understanding the interaction of five-membered aromatic heterocycles with Fe(110) surface is crucial for the development of novel inhibitors against the corrosion of iron and steel. Herein, we report a detailed study of the adsorption properties and the bonding mechanism of pyrrole, furan, and thiophene on Fe(110) surface employing density functional theory (DFT) calculations. In the most stable adsorption geometries, we found that the adsorbates lie flat at the hollow site and form chemical bondings with four Fe atoms on Fe(110) surface. The chemisorptions are indicated by large adsorption energies and charge transfers from the surface to the adsorbates. We also found that taking into account vdW corrections in the DFT calculations has a minimal effect on the adsorption geometries whereas it significantly increases the adsorption energies. The energetic and structural analysis reveals large molecular distortions induced by the adsorbate-surface interactions, and among the adsorbates, thiophene experiences the least molecular distortion, thereby having the largest adsorption energy. The electronic structure analysis also reveals that the nature of electronic interaction of pyrrole, furan, and thiophene with Fe(110) surface is due to the strong overlaps of the frontier  $\pi$  and  $\pi^*$  orbitals of the adsorbates with Fe- $3d_z^2$  and Fe- $(3d_{xz}+3d_{yz})$  states of the surface. The charge donation and back-donation between the adsorbates and Fe(110) surface were also elucidated by the Bader charge analysis and the charge density difference.

**Keywords:** five-membered ring; aromatic heterocycle; adsorption; charge transfer; vdW corrections; DFT; Fe(110) surface

## 1. Introduction

Understanding the interaction of five-membered aromatic heterocycles with metal surfaces<sup>1</sup> is not only of fundamental interest but also of practical importance to a wide range of applications, ranging from heterogeneous catalysis to corrosion protection. For instance, the adsorption of thiophene followed by the C–S bond rupture on transition metal surfaces is a key step in the mechanism of hydrodesulfurization.<sup>2-8</sup> The adsorption of furan on metal surfaces such as Pd and Pt are also of great importance in the catalytic conversion of furanic compounds to value-added chemical compounds.<sup>9-11</sup> Most importantly, the adsorption of five-membered aromatic heterocycles with Fe, Al, and Cu surfaces is very important to the inhibiting mechanism against the corrosion of these metals.<sup>12, 13</sup> Particularly, experimental studies have shown that organic molecules containing five-membered aromatic rings such as pyrrole (C<sub>4</sub>H<sub>4</sub>NH),<sup>14, 15</sup> furan (C<sub>4</sub>H<sub>4</sub>O),<sup>16, 17</sup> or thiophene (C<sub>4</sub>H<sub>4</sub>S)<sup>18-20</sup> are effective corrosion inhibitors for iron and steel in acidic media.

The inhibition performance of corrosion inhibitors is strongly correlated with the ability to get adsorbed on the metal surfaces. The lone pair of heteroatom (N, O, S) participates in the conjugated  $\pi$  bond system in the five-membered aromatic ring, and play a part in enhancing the inhibition efficiency of corrosion inhibitors. Nevertheless, the interaction mechanism of pyrrole, furan, and thiophene with corrosive metals such as Fe has not been thoroughly understood. The knowledge about the adsorption properties and bonding mechanism of pyrrole, furan, and thiophene on Fe surfaces is vital to understand the corrosion inhibiting mechanism, and thereby contributing to the development of novel corrosion inhibitors with better efficiency. Furthermore, as the simplest aromatic heterocycles, knowledge about the interaction mechanism of pyrrole, furan, and thiophene with Fe surfaces also provides a scientific

background for elucidating the bonding mechanism of more complex  $\pi$ -conjugated aromatic heterocycles with metal surfaces.

Density functional theory (DFT) has been proved as a useful tool for investigating the inhibiting mechanism of organic corrosion inhibitors.<sup>21, 22</sup> The interfacial properties of the inhibitor-metal systems dictating the inhibition efficiency such as the adsorption energy and the charge transfer could be provided by the results of the DFT calculations. The DFT studies on the adsorption mechanism of corrosion inhibitors have mainly focused on surfaces of Al<sup>23-</sup><sup>27</sup> and Cu<sup>28-34</sup>, and to our best knowledge, only a few studies to date have been conducted on Fe surfaces<sup>35-38</sup> despite the fact that Fe is the most used metal. Fe(110) is the most energetically stable surface among Fe surfaces,<sup>39</sup> therefore it was often chosen for the study of the adsorption mechanism. In a DFT study connected to the topic, Lei Guo and co-workers<sup>36</sup> calculated the adsorption energies of pyrrole, furan, and thiophene on Fe(110) surface to validate the empirical rule about the inhibition efficiency of organic inhibitors containing N, O, or S. In their work, however, the bonding mechanism of the adsorbates with the surface was not thoroughly investigated. Furthermore, the adsorption energies were calculated with standard DFT functionals such as PW91, PBE, and RPBE functionals, without taking into account the effect of van der Waals (vdW) interactions. Furthermore, it was pointed out by some DFT studies<sup>6, 7, 40, 41</sup> that the standard DFT functionals do not properly describe the interaction of aromatic ring molecules with metal surfaces, thus it is essential to perform vdW inclusive DFT calculations in the study of the adsorption of pyrrole, furan, and thiophene on Fe(110) surface.

In the present work, we perform a systematic study on the adsorption of pyrrole, furan, and thiophene on Fe(110) surface by means of DFT calculations, focusing on understanding the bonding mechanism of the adsorbates with the surface. The effect of vdW corrections on the adsorption properties was analyzed by comparing the adsorption energies and the adsorption

geometries by PBE functional with those by DFT-D3, optB88-vdW, and optB86b-vdW functionals. We also calculated and compared the energetic components constituting the adsorption energies of pyrrole, furan, and thiophene on Fe(110) surface. The electronic interactions of pyrrole, furan, and thiophene with Fe(110) surface were elucidated by examining the changes in the electronic structures of both the adsorbates and the surface upon the adsorptions. Besides, the charge donation and back-donation of the adsorbate-surface electronic interactions were also clarified by analyzing the charge density difference and the Bader charge calculations. Overall, our study provides insights into the bonding mechanism of pyrrole, furan, and thiophene with Fe(110) surface.

## 2. Computational methodology

The calculated lattice constant (2.82 Å) of a bcc Fe unit cell given by DFT calculations with PBE functionals were used for building Fe(110) surface. In this study, Fe(110) surface were modelled as a p(3x3) slab consisting of five atomic layers with a total of 45 Fe atoms. A vacuum space of 20 Å was included in the slab, above the topmost layer and along the z-direction, to alleviate the interactions between periodic images.

All spin-polarization DFT calculations were performed with the Vienna Ab initio Simulation Package (VASP 5.4.1)<sup>42-45</sup> using the projector augmented wave (PAW) method.<sup>46, 47</sup> The Perdew-Burke-Ernzerhof (PBE) exchange-correlation functional<sup>48</sup> within the framework of the generalized gradient approximation (GGA)<sup>49, 50</sup> were employed in the DFT calculations. The cut-off energy for the plane wave expansion was chosen to be 450 eV. The gamma-centered Monkhorst-Pack<sup>51</sup> with 5×5×1 and 6×6×1 k-point grids were employed to sample the Brillouin zone in the reciprocal space for the geometry optimizations and the electronic structure calculations respectively. The first order Methfessel-Paxton<sup>52</sup> smearing with  $\sigma=0.1$  eV was used to ensure convergence of the electronic relaxation, and the total energy has been extrapolated to 0 K. In the geometry optimizations, the adsorbates and the top two atomic layers

were allowed to relax to find their favourable positions whereas the bottom three layers were kept fixed in their bulk positions. The adsorption geometries were located by the conjugate gradient algorithm with a tight convergence threshold, that are  $10^{-8}$  eV for the electronic relaxation and  $0.01$  eV/Å for the Hellmann-Feynman force on each moving atom. Taking into account vdW interactions is very important in determining the interfacial properties of organic molecules on metal surfaces.<sup>53</sup> Therefore, the calculations were also carried out with vdW inclusive DFT methods, namely DFT-D3<sup>54</sup>, optB88-vdW, and optB86b-vdW<sup>55, 56</sup> functionals. The adsorption energy ( $E_{\text{ads}}$ ) of the molecules on Fe(110) surface was calculated as:

$$E_{\text{ads}} = E_{\text{molecule/Fe(110)}} - (E_{\text{molecule}} + E_{\text{Fe(110)}})$$

where  $E_{\text{Fe(110)}}$  is the total energy of a bare Fe(110) surface,  $E_{\text{molecule}}$  is the total energy of an optimized gas-phase molecule, and  $E_{\text{molecule/Fe(110)}}$  is the total energy of a molecule/Fe(110) system. A negative value of the adsorption energies indicates a favorable adsorption.

To better characterize the adsorbate-surface interactions, the adsorption energy were decomposed into three energetic components:

$$E_{\text{ads}} = E_{\text{mol-dist}} + E_{\text{surf-dist}} + E_{\text{int}}$$

The distortion energy of molecule (surface) is defined as the difference between the energy of an isolated molecule (surface) in a distorted geometry and the energy of an optimized gas-phase molecule (bare surface):

$$E_{\text{mol-dist}} = E_{\text{molecule(distorted)}} - E_{\text{molecule(gas-phase)}}.$$

$$E_{\text{surf-dist}} = E_{\text{surface(distorted)}} - E_{\text{surface(bare)}}.$$

The interaction energy ( $E_{\text{int}}$ ) between the molecules and Fe(110)surface was defined as:

$$E_{\text{int}} = E_{\text{molecule/Fe(110)}} - (E_{\text{molecule(distorted)}} + E_{\text{surface(distorted)}})$$

The electron density difference was calculated as:

$$\rho_{\text{CDD}} = \rho_{\text{molecule/Fe(110)}} - (\rho_{\text{molecule}} + \rho_{\text{Fe(110)}})$$

where  $\rho_{\text{molecule/Fe(110)}}$  indicates the electron density of a molecule/Fe(110) system, and  $\rho_{\text{molecule}}$  and  $\rho_{\text{Fe(110)}}$  represent the electron densities of the molecule and Fe(110) surface which are taken from the adsorption geometries respectively. The charge transfer from Fe(110) surface to the adsorbates were characterized by Bader charge analysis<sup>57</sup>, which was carried out with the computer program developed by Henkelman and co-workers.<sup>58-60</sup>

### 3. Results and Discussion

#### 3.1. Adsorption energies and equilibrium geometries

The main focus of this study is to give insights into the bonding mechanism of pyrrole, furan, and thiophene with Fe(110) surface, and the most stable adsorption geometries were required for the task. Fe(110) is a symmetric surface with a rhombus unit cell, having high-symmetry adsorption sites such as top, short-bridge, long-bridge, and hollow site. The hollow site has been shown as the most favourable site for the adsorption of aromatic ring molecules such as benzene<sup>61</sup> and phenol.<sup>41, 62</sup> Moreover, the adsorption of aromatic ring molecules on metal surfaces can occur via either a flat-lying (parallel) configuration or vertical (perpendicular) configuration, and the flat-lying geometry was found energetically more stable than the vertical geometry in the adsorption of thiophene<sup>6, 7</sup> and furan<sup>9</sup>. In other words, the adsorbate-substrate interaction is maximized when the aromatic ring plane lies flat on metal surfaces. Thus, the structural optimizations of pyrrole, furan, and thiophene on Fe(110) surface were started with the flat-lying geometries at the hollow site, and we found the most stable adsorption geometries as depicted in Fig.1. The adsorptions are driven by the chemical interactions of the five-membered aromatic rings with four Fe atoms around the hollow site including Fe(1) with the double bond C(1)=C(2), Fe(2) with the single bond C(2)-C(3), Fe(3) with the double bond C(3)=C(4), and Fe(4) with the heteroatom. We summarized the adsorption energies and adsorption bond lengths reported by PBE, DFT-D3, optB88-vdW, and optB86b-vdW functionals in Table 1. We note that bond lengths of the adsorption bonds are

comparable to the sum of covalent radii of participated atoms (Fe+C: 2.08 Å, Fe+N: 2.03 Å, Fe+O: 1.98 Å, and Fe+S: 2.37 Å),<sup>63</sup> indicating the covalent nature of the adsorption bonds. We also note that the adsorption geometries of pyrrole, furan, and thiophene on Fe(110) surface found by our study closely resemble those reported by Lei Guo et al.<sup>36</sup> The structural parameters in Table 2 present large molecular distortions by the chemical interactions with Fe(110) surface, and the most obvious changes are the expansions of the five-membered aromatic rings. It is worth noting that the elongation for the C=C double bonds is to a greater degree than for the C–C single bond which demonstrates a stronger interaction of the former with Fe(110) surface. We also notice that all the C–H bonds are tilted away from the ring plane (Fig.1). Most importantly, the chemical interactions with Fe(110) surface result in the buckling of the five-membered aromatic rings which can be recognized by the out-of-plane displacement of the heteroatom. As a result, the dihedral angles  $\angle X-C(1)-C(4)-C(2)$  and  $\angle X-C(1)-C(4)-C(3)$  of the adsorbates are less than those in free molecules ( $180^\circ$ ), and the degree of the ring buckling follows the order: thiophene < pyrrole < furan (Table 2). It is important to note that the interactions with Fe(110) surface cause pyrrole, furan, and thiophene are no longer planar molecules, thereby losing partly their aromaticity.

Furthermore, the chemisorptions of pyrrole, furan and thiophene on Fe(110) surface are indicated by large adsorption energies. From the DFT results with PBE functional, it can be seen that the adsorption energies of pyrrole (-1.16 eV) and furan (-1.17 eV) are almost equal while the adsorption energy of thiophene (-1.53 eV) is moderately greater. We found that the adsorption energies of pyrrole and furan are also comparable to the adsorption energy of benzene.<sup>61</sup> Taking account for vdW corrections results in slight reductions (within 0.05 Å) of the adsorption bond lengths whereas it significantly increases the adsorption energies. The adsorption energies of pyrrole, furan, and thiophene on Fe(110) surface given by used DFT functionals follow the increasing order PBE < optB88-vdW < DFT-D3 < optB86b-vdW. It

should be noted that a similar trend was also observed for the adsorption energies of six-membered aromatic compounds<sup>41</sup> on 3d, 4d, and 5d transition metal surfaces. We were unable to draw a direct benchmark comparison to evaluate how well each vdW-DFT functionals in describing the adsorbate-substrate interactions because of lacking the experimental adsorption energies of pyrrole, furan, and thiophene on Fe(110) surface. However, previous DFT studies<sup>41</sup> have found that DFT-D3 and optB86b-vdW functionals tend to overestimate the adsorption energies of aromatic ring compounds on transition metal surfaces while the adsorption energies given by optB88-vdW functional agree well with the experimental results. Thus, we only used PBE and optB88-vdW functionals in the remaining DFT calculations in this study.

The adsorption energy of the adsorbates on Fe(110) surface was decomposed into three energetic components, including the distortion energy of molecule ( $E_{\text{mol\_dist}}$ ), the distortion energy of surface ( $E_{\text{surf\_dist}}$ ), and the interaction energy ( $E_{\text{int}}$ ). We note from Table 3 that the adsorption energy of each adsorbate on the surface is a compromise between the destabilizing energies ( $E_{\text{mol\_dist}}$  and  $E_{\text{surf\_dist}}$ ) and the stabilizing energy ( $E_{\text{int}}$ ). To better visualize the correlation between the energetic components, the comparison between the adsorption energies and their energetic components is drawn in Figure 3. As can be seen, the distortion energies of surface are tiny (less than 0.1 eV) showing negligible distortions of Fe(110) surface induced by the adsorbate-surface interactions. By contrast, the distortion energies of molecules are large and follow the increasing order: thiophene < furan < pyrrole. It means that for effective adsorptions on Fe(110) surface, the adsorbates must overcome large distortion energies, and compared to benzene,<sup>61</sup> the distortion energies of pyrrole, furan, and thiophene are considerably larger. The distortion energies of molecule appear to be correlated with the degree of molecular distortions. Pyrrole has the largest distortion energies since it has one more C–H bond pointed away from the ring plane in combination with the second-largest ring buckling. By contrast, thiophene experiences the least ring buckling, thereby having the least distortion energies.

Taking into account for vdW corrections slightly change the distortion energies of both the adsorbates and the surface while it increases the interaction energies of pyrrole, furan, and thiophene with Fe(110) surface by 0.64, 0.57, and 0.78 eV respectively. It appears that the increase of the interaction energies by vdW corrections are consistent with the size of the molecules. It is worth mentioning that the interaction energies with Fe(110) surface of pyrrole, furan, and thiophene are approximately equal, thus among the adsorbates, thiophene has the greatest adsorption energy because it has the smallest distortion energy.

### 3.2. Electronic structure analysis

The bonding mechanism of aromatic ring molecules with transition metal surface has been discussed in several studies by analyzing the electronic structure of both the adsorbates and the substrates.<sup>3, 5, 6, 61, 64, 65</sup> Herein, by a similar approach, a detailed picture of the chemical bonding of pyrrole, furan, and thiophene with Fe(110) surface could be gained by scrutinizing the density of states (DOS), the charge density difference (CDD), and the result of Bader charge analysis. The adsorbate-substrate interactions cause changes in the electronic structures of both the adsorbates and the surface, particularly at the frontier electronic states. We note from Fig. 2 that the local density of states (LDOS) peaks corresponding to the highest occupied molecular orbitals (HOMO and HOMO-1,  $\pi$  orbitals) and the lowest unoccupied molecular orbital (LUMO and LUMO+1,  $\pi^*$  orbitals) are smeared out while the lower-energy LDOS peaks ( $\sigma$  orbitals) are just slightly broadened by the adsorbate-surface interactions. Fig. 2 also shows a good match between the electronic energies of the frontier  $\pi$  and  $\pi^*$  orbitals and Fe-3d states, and the electronic interactions of the adsorbates with Fe(110) surface occur the overlaps of these electronic states. The adsorptions on Fe(110) surface cause the buckling of the five-membered aromatic rings and thereby causing reductions of the HOMO-LUMO gap. The HOMO-LUMO gaps for pyrrole, furan and thiophene in the gas phase are 4.97, 4.73, and 4.47 eV while for isolated distorted molecules are reduced to 3.08, 2.92, and 3.00 eV respectively

(Table 3). The HOMO-LUMO gap is less reduced for thiophene (-1.47) than for pyrrole (-1.81) and furan (-1.89), which is consistent with the degree to which the five-membered aromatic rings are buckled by the adsorptions. It is interesting to note that the HOMO-LUMO gaps are reduced to approximately 3.00 eV, and it appears to be a good value for the electronic interactions between the five-membered aromatic heterocycles and Fe(110) surface. It should be recalled that the frontier  $\pi$  and  $\pi^*$  orbitals of pyrrole, furan, and thiophene are the linear combinations of  $2p_z$  orbitals of all the ring atoms. Accordingly, it is most likely that the frontier  $\pi$  and  $\pi^*$  orbitals primarily interact with Fe- $3d_z^2$  and Fe-( $3d_{xz}+3d_{yz}$ ) states owing to the matching of their symmetries. The electronic interactions could be clarified by examining the changes of the projected density of states (pDOS) of Fe- $3d_z^2$  and Fe-( $3d_{xz}+3d_{yz}$ ) electronic states. Fig.4 presents pDOS of  $3d_z^2$  and ( $3d_{xz}+3d_{yz}$ ) states of bonded Fe atoms on bare and adsorbed Fe(110) surfaces. In Fig.4a, the reduction of pDOS of Fe- $3d_z^2$  just below the Fermi level shows that Fe- $3d_z^2$  electronic state strongly hybridizes with the frontier  $\pi$  orbitals, creating the bonding states which is down-shifted below the bottom of Fe-3d band and antibonding states which is up-shifted to above the Fermi level. Moreover, the interaction with the frontier  $\pi^*$  orbital also contributes to the change of pDOS of Fe- $3d_z^2$ . Fig.4b also shows the changes of pDOS of Fe-( $3d_{xz}+3d_{yz}$ ) by the adsorbate-substrate interactions which exhibit a similar pattern with pDOS of Fe- $3d_z^2$ , although with less perturbation. Thus, the interactions of the frontier orbitals with Fe- $3d_z^2$  is stronger than with Fe-( $3d_{xz}+3d_{yz}$ ).

The CDD plots in Fig. 5 assist in characterizing the charge transfers between pyrrole, furan, and thiophene and Fe(110) surface. The charge accumulations at the spatial regions between the adsorbates and the surface clearly demonstrate the electronic interaction between them. The charge depletions at the five-member aromatic ring and the charge accumulation at Fe atoms exhibits the charge donation from the occupied  $\pi$  orbitals to Fe-3d states. By contrast, the charge accumulations at the regions above and outside the five-membered aromatic rings and

the charge depletions at Fe atoms exhibits the back-donation from Fe-3d states to the unoccupied  $\pi^*$  orbitals of the adsorbates. The depopulation of the bonding  $\pi$  orbitals by the charge donation and the population of the antibonding  $\pi^*$  orbitals by the back-donation are responsible for the elongations of all the ring bonds. The net effect of the charge donation and the back-donation is the charge transfer from Fe(110) surface to the adsorbates which can be quantified by the results of Bader charge analysis. Pyrrole, furan and thiophene gain a net charge of 0.75 e (0.72 e), 0.84 e (0.81 e), and 0.73 e (0.71 e) respectively from the substrate reported by PBE (optB88-vdW) functional. Furthermore, the electronic interactions with the adsorbates introduce changes in the electronic structure of Fe(110) surface. For instance, the d-band center of Fe atoms on the topmost layer is shifted toward higher binding energy. Besides, the average magnetic moment of Fe atoms on the topmost layer is also reduced by about 0.18 to 0.25  $\mu_B$  (Table 4) due to the adsorbate-substrate interactions.

#### **4. Conclusions**

We have presented a systematic study on the adsorption properties and bonding mechanism of pyrrole, furan, and thiophene on Fe(110) surface based on DFT results with PBE, DFT-D3, optB88-vdW, and optB86b-vdW functionals. We found from the geometry optimizations that pyrrole, furan, and thiophene prefer binding with Fe(110) surface at the hollow site and in the flat-lying geometries. The adsorptions are driven by the formation of covalent bonds between the ring atoms and four surface Fe atoms. We note that taking into account for vdW corrections have a small effect on the adsorption geometries whereas it significantly increases the calculated adsorption energies. DFT calculated results show large adsorption energies and large charge transfers from Fe(110) surface to pyrrole, furan, and thiophene, indicating the chemisorption of pyrrole, furan, and thiophene on the surface. The chemisorption on Fe(110) surface results in the elongations of all the ring bonds and the out-of-plane displacements of both the C–H bonds and the heteroatom. Among the adsorbates,

thiophene experiences the least molecular distortion upon the adsorption on Fe(110) surface, causing it to have the largest adsorption energies although the adsorbate-surface interaction energies are comparable for all the adsorbates. The pDOS analysis reveals that the electronic interactions occur by the overlaps of the frontier  $\pi$  and  $\pi^*$  orbitals of the adsorbates and Fe-3d<sup>2</sup> and Fe-(3d<sub>xz</sub>+3d<sub>yz</sub>) states of Fe(110) surface. We also found from the CDD analysis that the adsorbate-substrate interactions give rise to the charge donation from the occupied  $\pi$  orbitals to unfilled Fe-3d states and the back-donation from filled Fe-3d states to the empty  $\pi^*$  orbitals.

### **Conflicts of Interest**

The authors declare that there are no conflicts of interest regarding the publication of this paper.

### **Acknowledgment**

This research is funded by Vietnam National Foundation for Science and Technology Development (NAFOSTED) under grant number 103.01-2017.370.

**Table 1.** Adsorption energies and bond lengths of the adsorption bonds on Fe(110) surface.

Adsorption system	DFT functional	$E_{\text{ads}}$ (eV)	Bond distance ( $\text{\AA}$ )						
			Fe(1)–C(1)	Fe(1)–C(2)	Fe(2)–C(2)	Fe(2)–C(3)	Fe(3)–C(3)	Fe(3)–C(4)	Fe(4)–X
Pyrrole/ Fe(110)	PBE	-1.16	2.01	2.18	2.25	2.26	2.16	2.01	2.01
	DFT-D3	-2.03	2.01	2.16	2.25	2.26	2.15	2.01	2.00
	optB88- vdW	-1.86	2.01	2.21	2.23	2.28	2.16	2.00	2.00
	optB86b- vdW	-2.27	1.99	2.17	2.23	2.26	2.15	1.99	1.99
Furan/ Fe(110)	PBE	-1.17	2.00	2.18	2.24	2.23	2.18	2.00	2.11
	DFT-D3	-1.93	1.99	2.17	2.24	2.23	2.17	1.99	2.10
	optB88- vdW	-1.82	1.99	2.19	2.25	2.25	2.20	1.99	2.09
	optB86b- vdW	-2.20	1.98	2.15	2.24	2.23	2.15	1.98	2.07
Thiophene/ Fe(110)	PBE	-1.53	1.99	2.30	2.21	2.21	2.30	1.99	2.21
	DFT-D3	-2.45	1.98	2.27	2.20	2.20	2.27	1.98	2.21
	optB88- vdW	-2.33	1.99	2.29	2.22	2.22	2.29	1.98	2.22
	optB86b- vdW	-2.72	1.98	2.25	2.20	2.20	2.25	1.98	2.20

**Table 2.** Structural parameters and HOMO-LUMO gap of free and isolated distorted pyrrole, furan, and thiophene.

Molecule	Bond length (Å)					Dihedral angle (°)		HOMO-LUMO gap
	C(1)–C(2)	C(2)–C(3)	C(3)–C(4)	C(4)–X	C(1)–X	∠X-C(1)-C(4)-C(2)	∠X-C(1)-C(4)-C(3)	
free pyrrole	1.38	1.42	1.38	1.38	1.38	180.00	180.00	4.97
distorted pyrrole	1.47	1.49	1.47	1.47	1.47	173.95	173.90	3.08
free furan	1.36	1.43	1.36	1.37	1.37	180.00	180.00	4.73
distorted furan	1.46	1.48	1.46	1.47	1.47	165.40	165.41	2.92
free thiophene	1.38	1.42	1.38	1.71	1.72	180.00	180.00	4.47
distorted thiophene	1.47	1.47	1.47	1.82	1.82	176.47	176.48	3.00

**Table 3.** Adsorption energy, distortion energy of molecule ( $E_{\text{mol\_dist}}$ ), distortion energy of surface ( $E_{\text{surf\_dist}}$ ), and interaction energy ( $E_{\text{int}}$ ).

<b>Adsorption system</b>	<b>DFT functional</b>	<b><math>E_{\text{ads}}</math> (eV)</b>	<b><math>E_{\text{mol\_dist}}</math> (eV)</b>	<b><math>E_{\text{surf\_dist}}</math> (eV)</b>	<b><math>E_{\text{int}}</math> (eV)</b>
Pyrrole /Fe(110)	PBE	-1.16	2.40	0.07	-3.63
	optB88-vdW	-1.86	2.33	0.07	-4.27
Furan /Fe(110)	PBE	-1.17	2.36	0.07	-3.60
	optB88-vdW	-1.82	2.28	0.07	-4.17
Thiophene /Fe(110)	PBE	-1.53	1.88	0.09	-3.50
	optB88-vdW	-2.33	1.86	0.09	-4.28

**Table 4.** Charge transfer from Fe(110) surface to the adsorbates and change of d-band center and magnetic moment of the topmost layer Fe atoms on Fe(110) surface by the adsorptions.

<b>Adsorption system</b>	<b>DFT functional</b>	<b>charge transfer (e)</b>	<b><math>\Delta E_d</math> (eV)</b>	<b><math>\Delta\mu</math> (<math>\mu_B</math>)</b>
Pyrrole /Fe(110)	PBE	0.75	-0.10	-0.21
	optB88-vdW	0.72	-0.09	-0.23
Furan /Fe(110)	PBE	0.84	-0.08	-0.18
	optB88-vdW	0.81	-0.07	-0.18
Thiophene /Fe(110)	PBE	0.73	-0.09	-0.25
	optB88-vdW	0.71	-0.08	-0.25

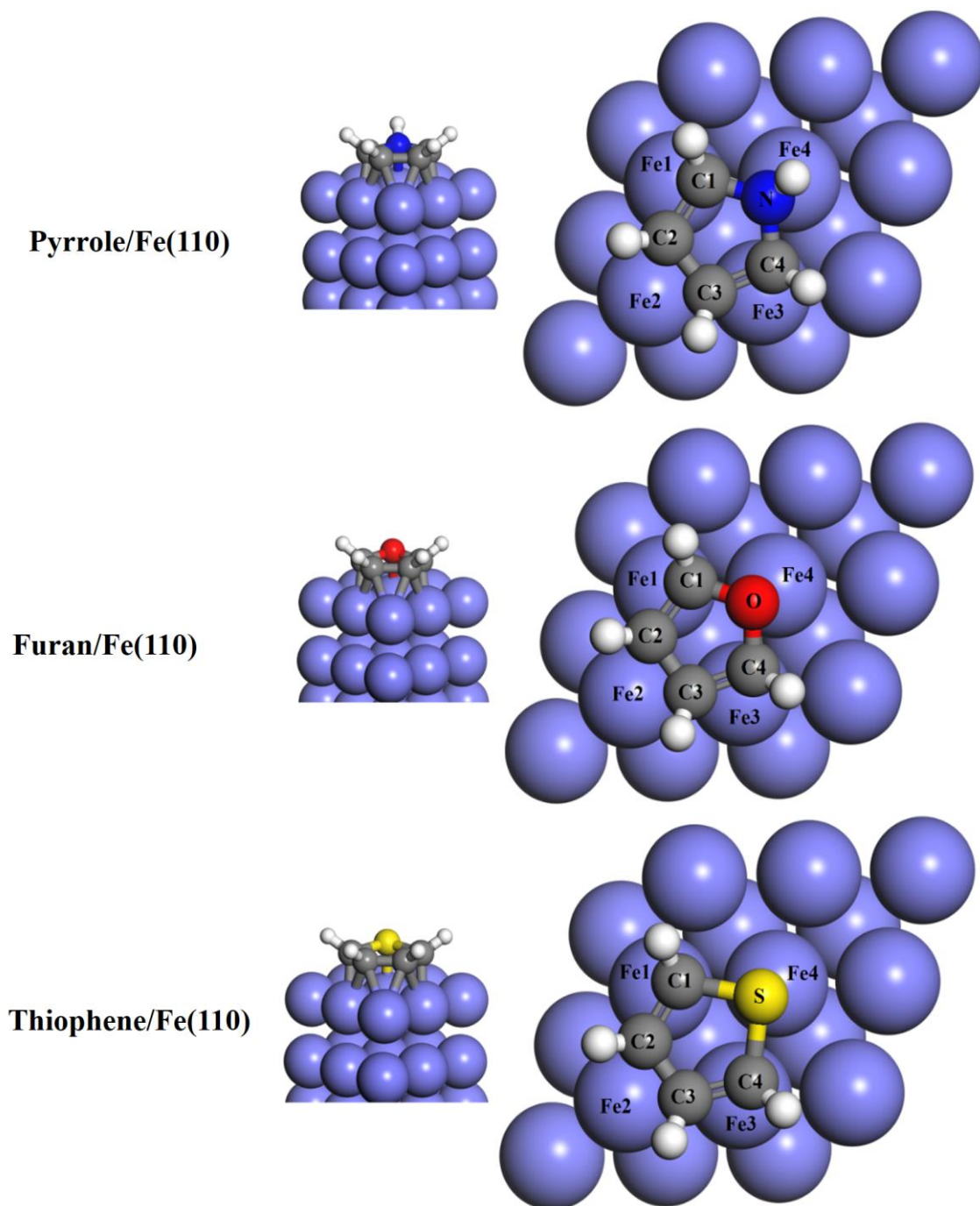


**Fig. 1.** The most stable adsorption geometries.

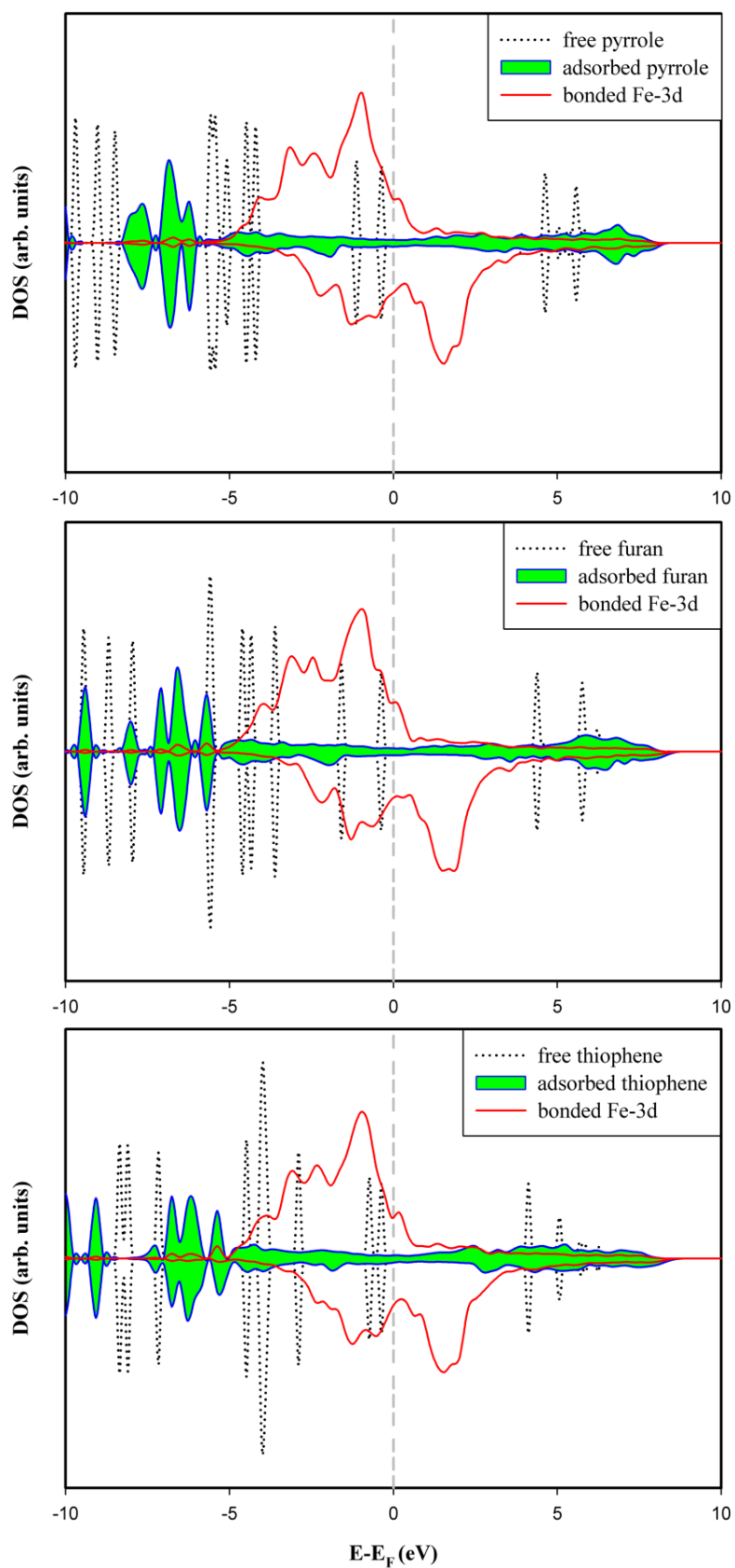


**Fig. 2.** The local density of states of free, adsorbed adsorbates and bonded Fe-3d.

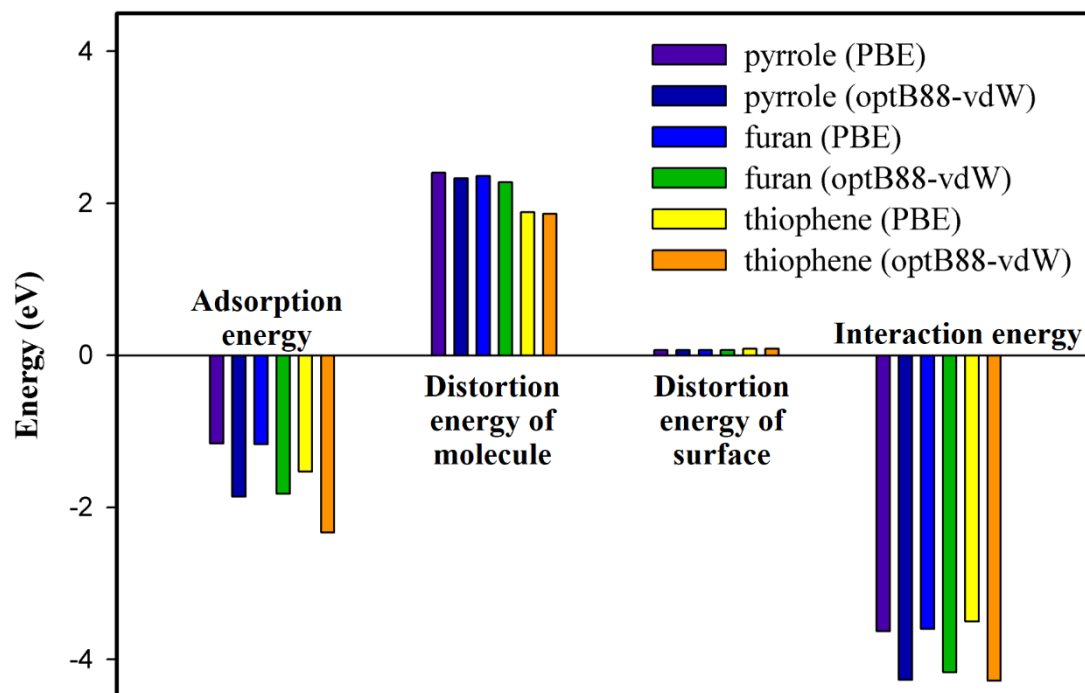


**Fig. 3.** The comparison between the adsorption energies, the energies of molecular distortion, the energies of surface distortion, and the energies of adsorbate-surface interaction

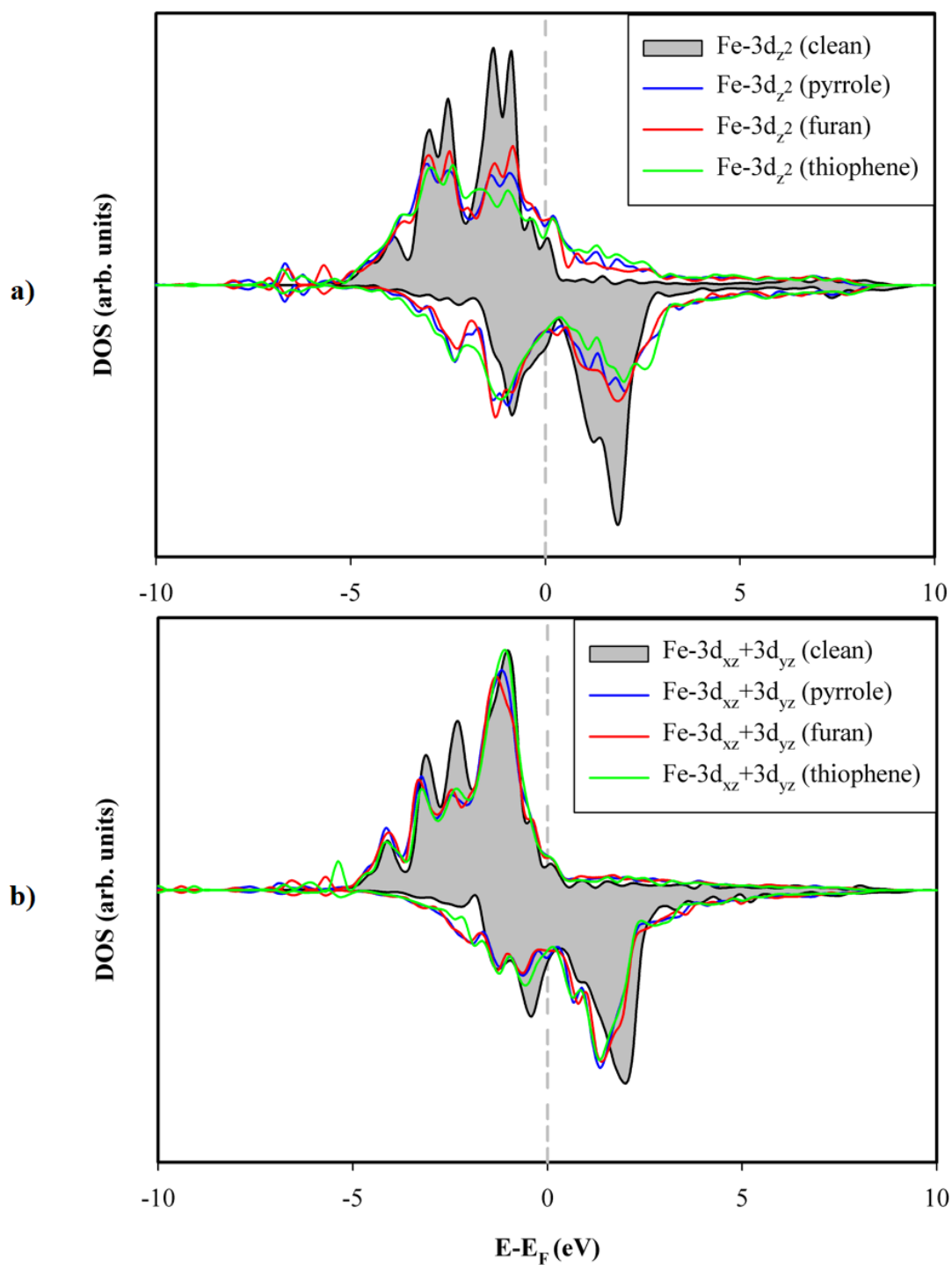


**Fig. 4.** The projected density of states of Fe- $3d_{z^2}$  and Fe-( $3d_{xz}+3d_{yz}$ ) for clean and adsorbed Fe(110) surfaces.

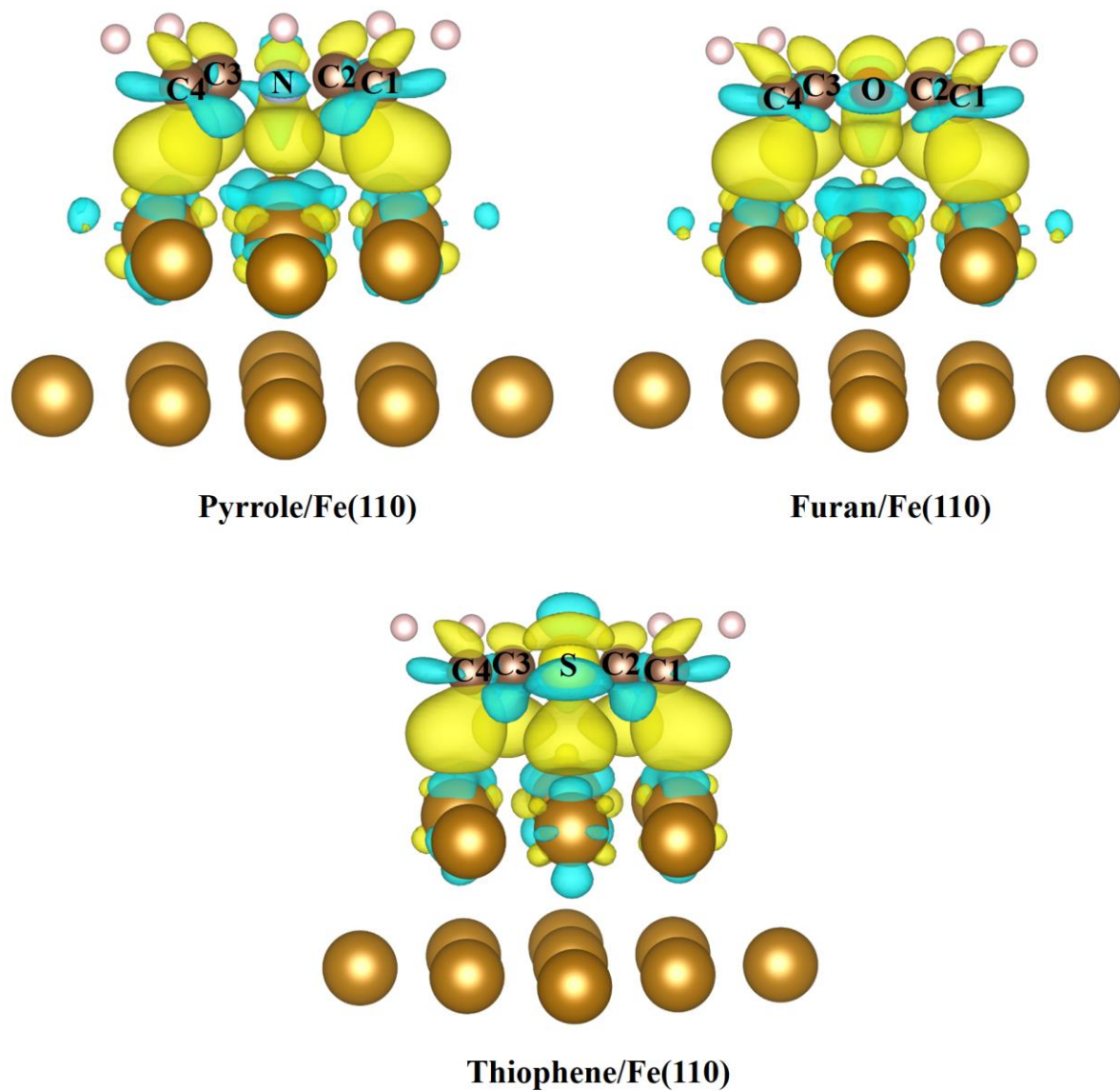


**Fig. 5.** The plots of charge density difference for the adsorbate/Fe(110) systems. The isosurface is taken as  $0.008 \text{ e/Bohr}^3$ . The yellow color and the light green color represent the electron accumulations and electron depletions respectively.

## References

1. S. J. Jenkins, *Proceedings of the Royal Society A: Mathematical, Physical and Engineering Sciences*, 2009, **465**, 2949-2976.
2. H. Zhu, W. Guo, M. Li, L. Zhao, S. Li, Y. Li, X. Lu and H. Shan, *ACS Catalysis*, 2011, **1**, 1498-1510.
3. F. Mittendorfer and J. Hafner, *Journal of Catalysis*, 2003, **214**, 234-241.
4. C. Morin, A. Eichler, R. Hirschl, P. Sautet and J. Hafner, *Surface Science*, 2003, **540**, 474-490.
5. F. Mittendorfer and J. Hafner, *Surface Science*, 2001, **492**, 27-33.
6. W. Malone, H. Yildirim, J. Matos and A. Kara, *The Journal of Physical Chemistry C*, 2017, **121**, 6090-6103.
7. W. Malone, J. Matos and A. Kara, *Surface Science*, 2018, **669**, 121-129.
8. W. Malone, W. Kaden and A. Kara, *Surface Science*, 2019, **686**, 30-38.
9. S. Wang, V. Vorotnikov and D. G. Vlachos, *Green Chemistry*, 2014, **16**, 736-747.
10. A. Loui and S. Chiang, *Surface Science*, 2018, **670**, 13-22.
11. L. O. Mark, N. Agrawal, A. M. Román, A. Holewinski, M. J. Janik and J. W. Medlin, *ACS Catalysis*, 2019, **9**, 11360-11370.
12. M. Goyal, S. Kumar, I. Bahadur, C. Verma and E. E. Ebenso, *Journal of Molecular Liquids*, 2018, **256**, 565-573.
13. C. Verma, L. O. Olasunkanmi, E. E. Ebenso and M. A. Quraishi, *Journal of Molecular Liquids*, 2018, **251**, 100-118.
14. M. Dūdükü, B. Yazici and M. Erbil, *Materials Chemistry and Physics*, 2004, **87**, 138-141.
15. G. Moretti, G. Quartarone, A. Tassan and A. Zingales, *Materials and Corrosion*, 1994, **45**, 641-647.
16. E. Machnikova, K. H. Whitmire and N. Hackerman, *Electrochimica Acta*, 2008, **53**, 6024-6032.
17. K. F. Khaled, *Journal of The Electrochemical Society*, 2010, **157**, C116.
18. Z. Szklarska-smialowska and M. Kaminski, *Corrosion Science*, 1973, **13**, 1-10.
19. M. Bouklah, B. Hammouti, A. Aouniti and T. Benhadda, *Progress in Organic Coatings*, 2004, **49**, 225-228.
20. M. Bouklah, B. Hammouti, M. Benkaddour and T. Benhadda, *Journal of Applied Electrochemistry*, 2005, **35**, 1095-1101.
21. E. Ebenso, C. Verma, L. Olasunkanmi, E. D. Akpan, D. Verma, H. Lgaz, L. Guo, S. Kaya and M. A. Quraishi, *Physical Chemistry Chemical Physics*, 2021.
22. A. Kokalj, *Corrosion Science*, 2021, 109650.
23. F. Chiter, C. Lacaze-Dufaure, H. Tang and N. Pébère, *Physical Chemistry Chemical Physics*, 2015, **17**, 22243-22258.
24. F. Chiter, M.-L. Bonnet, C. Lacaze-Dufaure, H. Tang and N. Pébère, *Physical Chemistry Chemical Physics*, 2018, **20**, 21474-21486.
25. Y. Bulteau, N. Tarrat, N. Pébère and C. Lacaze-Dufaure, *New Journal of Chemistry*, 2020, **44**, 15209-15222.
26. H. Allal, Y. Belhocine and E. Zouaoui, *Journal of Molecular Liquids*, 2018, **265**, 668-678.
27. D. Costa, T. Ribeiro, P. Cornette and P. Marcus, *The Journal of Physical Chemistry C*, 2016, **120**, 28607-28616.
28. A. Kokalj and S. Peljhan, *Langmuir*, 2010, **26**, 14582-14593.
29. S. Peljhan and A. Kokalj, *Physical Chemistry Chemical Physics*, 2011, **13**, 20408-20417.

30. A. Kokalj, S. Peljhan, M. Finšgar and I. Milošev, *Journal of the American Chemical Society*, 2010, **132**, 16657-16668.
31. N. Kovačević and A. Kokalj, *Corrosion Science*, 2013, **73**, 7-17.
32. C. Gattinoni and A. Michaelides, *Faraday Discussions*, 2015, **180**, 439-458.
33. N. Kovačević, I. Milošev and A. Kokalj, *Corrosion Science*, 2017, **124**, 25-34.
34. S. Sun, Y. Geng, L. Tian, S. Chen, Y. Yan and S. Hu, *Corrosion Science*, 2012, **63**, 140-147.
35. J. Radilla, G. E. Negrón-Silva, M. Palomar-Pardavé, M. Romero-Romo and M. Galván, *Electrochimica Acta*, 2013, **112**, 577-586.
36. L. Guo, I. B. Obot, X. Zheng, X. Shen, Y. Qiang, S. Kaya and C. Kaya, *Applied Surface Science*, 2017, **406**, 301-306.
37. M. Özcan, D. Toffoli, H. Üstünel and İ. Dehri, *Corrosion Science*, 2014, **80**, 482-486.
38. D. Kumar, V. Jain and B. Rai, *Corrosion Science*, 2018, **142**, 102-109.
39. P. Błoński and A. Kiejna, *Surface Science*, 2007, **601**, 123-133.
40. H. Yildirim, T. Greber and A. Kara, *The Journal of Physical Chemistry C*, 2013, **117**, 20572-20583.
41. X. Jia and W. An, *The Journal of Physical Chemistry C*, 2018, **122**, 21897-21909.
42. G. Kresse and J. Hafner, *Physical Review B*, 1993, **47**, 558-561.
43. G. Kresse and J. Hafner, *Physical Review B*, 1994, **49**, 14251-14269.
44. G. Kresse and J. Furthmüller, *Physical Review B*, 1996, **54**, 11169-11186.
45. G. Kresse and J. Furthmüller, *Computational Materials Science*, 1996, **6**, 15-50.
46. G. Kresse and D. Joubert, *Physical Review B*, 1999, **59**, 1758-1775.
47. P. E. Blöchl, *Physical Review B*, 1994, **50**, 17953-17979.
48. J. P. Perdew, K. Burke and M. Ernzerhof, *Physical Review Letters*, 1996, **77**, 3865-3868.
49. J. P. Perdew, J. A. Chevary, S. H. Vosko, K. A. Jackson, M. R. Pederson, D. J. Singh and C. Fiolhais, *Physical Review B*, 1992, **46**, 6671-6687.
50. A. D. Becke, *Physical Review A*, 1988, **38**, 3098-3100.
51. H. J. Monkhorst and J. D. Pack, *Phys. Rev. B*, 1976, **13**, 5188.
52. M. Methfessel and A. T. Paxton, *Physical Review B*, 1989, **40**, 3616-3621.
53. D. Yuan, Y. Zhang, W. Ho and R. Wu, *The Journal of Physical Chemistry C*, 2020, **124**, 16926-16942.
54. S. Grimme, J. Antony, S. Ehrlich and H. Krieg, *The Journal of Chemical Physics*, 2010, **132**, 154104.
55. J. Klimeš, D. R. Bowler and A. Michaelides, *Journal of Physics: Condensed Matter*, 2009, **22**, 022201.
56. J. Klimeš, D. R. Bowler and A. Michaelides, *Physical Review B*, 2011, **83**, 195131.
57. R. F. W. Bader, *Chemical Reviews*, 1991, **91**, 893-928.
58. W. Tang, E. Sanville and G. Henkelman, *Journal of Physics: Condensed Matter*, 2009, **21**, 084204.
59. E. Sanville, S. D. Kenny, R. Smith and G. Henkelman, *Journal of Computational Chemistry*, 2007, **28**, 899-908.
60. G. Henkelman, A. Arnaldsson and H. Jónsson, *Computational Materials Science*, 2006, **36**, 354-360.
61. A. J. R. Hensley, R. Zhang, Y. Wang and J.-S. McEwen, *The Journal of Physical Chemistry C*, 2013, **117**, 24317-24328.
62. A. J. R. Hensley, Y. Wang and J.-S. McEwen, *Surface Science*, 2014, **630**, 244-253.
63. P. Pykkö and M. Atsumi, *Chemistry – A European Journal*, 2009, **15**, 186-197.
64. F. Mittendorfer and J. Hafner, *Surface Science*, 2001, **472**, 133-153.

65. C. Morin, D. Simon and P. Sautet, *The Journal of Physical Chemistry B*, 2004, **108**, 12084-12091.